

# Theoretical investigation on the liquid junction potential in a slit-like microchannel

Kwan Hyoung Kang <sup>a,\*</sup>, In Seok Kang <sup>b</sup>

<sup>a</sup> Department of Mechanical Engineering, Pohang University of Science and Technology, San 31, Hyoja-dong, Pohang 790-784, Republic of Korea

<sup>b</sup> Department of Chemical Engineering, Pohang University of Science and Technology, San 31, Hyoja-dong, Pohang 790-784, Republic of Korea

Received 30 July 2003; received in revised form 3 October 2003; accepted 20 November 2003

## Abstract

A liquid junction potential (LJP) is generated at the interface of the two electrolyte solutions of different ionic concentrations. It can be applied to generate electricity and it can also be applied to passive control of the trajectory of the charged micro- and nanoparticles in micro total analysis systems. In this article, an analytical model is provided to predict the LJP and the associated electrostatic field generated by the two contacting electrolyte layers in a slit-like channel, for the case of the simple 1:1 electrolyte system. The one-dimensional Nernst–Planck equation is analyzed to investigate the temporal evolution of the concentration distribution. As a result, comprehensive analytical formulas for the LJP, the electric field, and the charge density are obtained. The LJP is obtained by introducing the concentrations at the boundary surfaces to Planck's equation written for the finite domain. The analytical result for the LJP is compared with the existing experimental result, which shows a reasonable agreement. Of particular interest is the influence of the initial concentration ratio and the thickness ratio of the two electrolyte layers. It is shown that there exist limiting profiles in the temporal evolution of the LJP, with respect to the variation of the concentration ratio and the thickness ratio, respectively. The implication of the electric field produced by the charge separation is discussed concerning the behavior of the charged particles in micro total analysis systems.

© 2003 Elsevier B.V. All rights reserved.

**Keywords:** Liquid junction; Diffusion; Electric potential; Channel flow; Fuel cell

## 1. Introduction

The liquid junction potential (LJP) arises at the interface of two liquid electrolyte layers due to separation of the electrical charges which is basically induced by the difference in ionic mobility [1]. The LJP can be used to generate electricity in a microscale channel (micro-channel) by beneficial usage of the laminar flow and subsequent slow-mixing character in very small dimensions [2–4]. Another application of the LJP is to use it for the determination of equilibrium constants by means of the potentiometric technique [5].

The liquid interfaces of miscible or immiscible fluids appear frequently in micro total analysis systems ( $\mu$ TASs) in mixing and separation processes [6–8]. In the

$\mu$ TASs, the LJP could cause a significant problem by inducing spurious electrophoretic transport of analytes. This characteristic can be beneficially utilized to concentrate or separate charged species based on their mobilities [6]. In another aspect, an interesting instability mode occurs at the interface of the two miscible electrolyte solutions (of different concentrations) for the slow electro-osmotically driven flow in a T-channel [7]. The mechanism of the instability remains unknown. It is believed that the charge separation and the subsequent appearance of the electric field due to the LJP play a substantial role in the appearance of the instability.

The mean translation distance of molecules per unit time is in the order of  $\sqrt{D}$ , where  $D$  is the molecular diffusivity which has a typical value of  $10^{-9}$  m<sup>2</sup>/s. Therefore, the diffusion time required to translate the mean distance of  $l_c$  is of the order of  $l_c^2/D$ . For a macroscopic system in which  $l_c$  is usually greater than 1 cm, the diffusion time is of the order of hours. Accordingly,

\* Corresponding author. Tel.: +82-54-279-8201; fax: +82-54-279-3199.

E-mail address: [khkang@postech.edu](mailto:khkang@postech.edu) (K.H. Kang).

within a moderate time, the system can be regarded as an infinite (unbounded) system. Most previous investigations concerning the temporal evolution of the LJP, in the case where the two electrolyte solutions are in direct contact, have dealt with infinite systems, theoretically [9–11] and numerically [12].

On the other hand, for the microscopic systems, such as the microchannel in the  $\mu$ TAS in which  $l_c$  is usually less than 100  $\mu\text{m}$ , the diffusion time is of the order of a few seconds. Many important processes in  $\mu$ TAS occur on this time scale. Accordingly, the charge separation process and the detailed character of the LJP in a micro system can be much different from that of the infinite domain. This is because the diffusion and the electrostatic field are strongly influenced by the bounding surfaces of the system, and also, the total amount of a species is finite, so that the mixing process will finish within a finite time.

There are two recent papers of Munson et al. [6] and Josserand et al. [3] which have considered the finiteness of the domain for LJP-related problems. Munson et al. [6] have shown that the LJP formed in microchannels can induce appreciable electrophoretic transport of charged species without the use of electrodes and an external power supply. To predict the mass transport, they introduced a 1-D numerical model for the Nernst–Planck equation under the electroneutrality assumption, which shows a qualitative agreement with their own experimental data. Josserand et al. [3] may be the first who have specifically considered the magnitudes of the LJP in the microchannel geometry. They performed a 2-D numerical simulation under a similar framework to that of Munson et al. [6]. They obtained the LJP by applying Planck's equation, which shows reasonable agreement with their own experimental results.

In the present investigation, we provide a 1-D theoretical model for a similar system without considering the convection effect. Negligence of the convection effect will be justified for the case of the electro-osmotically driven flows in which the velocity profile is almost uniform. The streamwise coordinate is replaced by the pseudo-time, as was done by Munson et al. [6]. Then, the time-dependent diffusion of species is predicted analytically and is validated numerically. Following the previous work [3,6], we introduce the Nernst–Planck equation and the electroneutrality assumption to correlate the concentration distribution to the electric field. Of particular interest are the effects of the initial concentration ratio and the initial thickness ratio of the two liquid layers. As will be shown, the analytical results manifest rich dynamic features of this fundamentally important problem. Among them, we obtain the maximum attainable open-circuit voltage of the system for a given initial concentration ratio and initial thickness ratio.

The LJP obtained by the present theory is compared to the experimental results of Josserand et al. [3] to

check the applicability of the theory to the flowing system, which shows a reasonable agreement. Nevertheless, the present theoretical model may not be superior in quantitative prediction of the LJP (due to the simplification made for the analytical treatment of the problem) to the numerical results for a specific case of a flowing system. However, it can constitute a backbone for deeper understanding of the phenomena, and it will provide useful insight into any future explanation of the instability mechanism of Chen and Santiago [7].

## 2. Analysis

### 2.1. Basic equations

We consider the time-dependent mixing of two 1:1 symmetric electrolyte layers of initially different concentrations contained in a two-dimensional slit-like channel (see Fig. 1). The composition of the two electrolyte layers is assumed to be the same. The electrolytes are free from chemical reaction. The dielectric constant of the solution is assumed to be constant independent of position. For simplicity of analysis, the activity coefficient is assumed to be unity. This assumption is justified for the case of infinite dilution.

The channel height is denoted by  $d$ , and the channel extends to infinity in the positive and the negative directions. The initial concentrations are denoted by  $c_{h0}$  and  $c_{l0}$ , in which 'h' and 'l' mean the high and low concentrations. The thicknesses of the diluted and concentrated solutions are different and denoted by  $d_l$  and  $d_h$ , respectively. The two electrolyte layers are initially prevented from mixing by an imaginary barrier. After removing the barrier, the ions diffuse and mixing takes place.

Hereinafter, the subscripts 1 and 2 indicate the positive ions (cations) and the negative ions (anions), respectively. The conservation equation for each ionic species is written as

$$\frac{\partial c_i}{\partial t} + \nabla \cdot \mathbf{j}_i = 0, \quad (1)$$

where  $i = 1$  and 2 denote the ionic species,  $c_i$  is the molar concentration ( $\text{mol}/\text{m}^3$ ), and  $t$  is the time. If we assume Fickian diffusion of the species, the current density  $\mathbf{j}_i$  is written as the sum of diffusional, electromigrational, and convective components as follows:

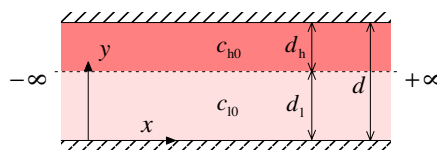


Fig. 1. Two electrolyte layers in a two dimensional slit-like channel. The two layers have the same composition but different initial concentrations of  $c_{h0}$  and  $c_{l0}$ .

$$\mathbf{j}_i = -D_i \nabla c_i + z_i \omega_i F c_i \mathbf{E} + c_i \mathbf{u}. \quad (2)$$

Here,  $D_i$  is the diffusivity of the ionic species ( $\text{m}^2/\text{s}$ ),  $z_i$  is the valence of the ionic species which is chosen as unity in this work,  $F = N_A e = 9.65 \times 10^4 \text{ C/mol}$  is the Faraday constant,  $N_A = 6.022 \times 10^{23}/\text{mol}$  is the Avogadro number,  $e = 1.602 \times 10^{-19} \text{ C}$  is the electronic charge,  $\mathbf{E} = -\nabla \phi$  is the electric field,  $\phi$  is the electrostatic potential,  $\omega_i$  is the mobility of the ionic species ( $\text{mol m N}^{-1} \text{ s}^{-1}$ ) and  $\mathbf{u}$  is the convection velocity. According to the Einstein relation [13], the mobility is related to the diffusivity as

$$\omega_i = \frac{D_i}{RT} = \frac{D_i}{N_A K T} \quad (3)$$

in which  $R = KN_A = 8.314 \text{ J/mol K}$  is the ideal gas constant,  $k = 1.38 \times 10^{-23} \text{ J/K}$  is the Boltzmann constant, and  $T$  is the absolute temperature (K). The electrostatic potential  $\phi$  is related to the charge density ( $\rho_e$ ) by the following Poisson equation.

$$\nabla^2 \phi = -\frac{\rho_e}{\varepsilon} = \frac{F}{\varepsilon} (c_2 - c_1), \quad (4)$$

where  $\varepsilon$  is the electric permittivity.

We consider the case of a quiescent liquid so that we neglect the convective current in Eq. (2). Then, the one-dimensional ion transport equations for each species and the Poisson equation become

$$\frac{\partial c_1}{\partial t} = D_1 \left[ \frac{\partial^2 c_1}{\partial y^2} + \frac{F}{RT} \frac{\partial}{\partial y} \left( c_1 \frac{\partial \phi}{\partial y} \right) \right], \quad (5a)$$

$$\frac{\partial c_2}{\partial t} = D_2 \left[ \frac{\partial^2 c_2}{\partial y^2} - \frac{F}{RT} \frac{\partial}{\partial y} \left( c_2 \frac{\partial \phi}{\partial y} \right) \right], \quad (5b)$$

$$\frac{\partial^2 \phi}{\partial y^2} = -\frac{\rho_e}{\varepsilon} = \frac{F}{\varepsilon} (c_2 - c_1). \quad (6)$$

The initial condition and the boundary condition for  $c_1$ ,  $c_2$ , and  $\phi$  are written as

$$c_{1,2}(t = 0, y) = \begin{cases} c_{l0} & \text{if } y < d_1, \\ c_{h0} & \text{if } y > d_1, \end{cases} \quad (7)$$

$$\frac{\partial c_{1,2}}{\partial y} \Big|_{y=0} = \frac{\partial c_{1,2}}{\partial y} \Big|_{y=d} = 0, \quad (8a)$$

$$\frac{\partial \phi}{\partial y} \Big|_{y=0} = \frac{\partial \phi}{\partial y} \Big|_{y=d} = 0. \quad (8b)$$

## 2.2. Non-dimensionalization

For the sake of convenience, we introduce the following non-dimensional variables

$$\tau = \frac{t}{d^2/D_{\text{eq}}}, \quad \eta = \frac{y}{d}, \quad \varphi = \beta \phi, \quad C_i = \frac{c_i}{c_{h0} - c_{l0}}, \quad (9)$$

where  $\beta = F/RT$ , and  $D_{\text{eq}}$  is the equivalent diffusivity which is defined as follows:

$$D_{\text{eq}} = \frac{2D_1 D_2}{D_1 + D_2}. \quad (10)$$

By substituting the dimensionless variables in Eqs. (5a), (5b) and (6), we obtain the following non-dimensional equations

$$\frac{\partial C_1}{\partial \tau} = \frac{D_1}{D_{\text{eq}}} \left[ \frac{\partial^2 C_1}{\partial \eta^2} + \frac{\partial}{\partial \eta} \left( C_1 \frac{\partial \varphi}{\partial \eta} \right) \right], \quad (11a)$$

$$\frac{\partial C_2}{\partial \tau} = \frac{D_2}{D_{\text{eq}}} \left[ \frac{\partial^2 C_2}{\partial \eta^2} - \frac{\partial}{\partial \eta} \left( C_2 \frac{\partial \varphi}{\partial \eta} \right) \right], \quad (11b)$$

$$\frac{\partial^2 \varphi}{\partial \eta^2} = (\kappa d)^2 (C_2 - C_1), \quad (12)$$

where  $\kappa$  is the inverse Debye length which is defined as follows:

$$\kappa^2 = \frac{F^2 (c_{h0} - c_{l0})}{\varepsilon RT}. \quad (13)$$

The initial condition and the boundary condition written for the dimensionless concentration ( $C_{1,2}$ ) and the electrostatic potential ( $\varphi$ ) becomes

$$C_{1,2}(\tau = 0, \eta) = \begin{cases} \frac{c_{l0}}{c_{h0} - c_{l0}} & \text{if } \eta < \xi, \\ \frac{c_{h0}}{c_{h0} - c_{l0}} & \text{if } \eta > \xi, \end{cases} \quad (14)$$

$$\frac{\partial C_{1,2}}{\partial \eta} \Big|_{\eta=0} = \frac{\partial C_{1,2}}{\partial \eta} \Big|_{\eta=1} = 0, \quad (15a)$$

$$\frac{\partial \varphi}{\partial \eta} \Big|_{\eta=0} = \frac{\partial \varphi}{\partial \eta} \Big|_{\eta=1} = 0, \quad (15b)$$

where  $\xi = d_i/d$  denotes the dimensionless position of the interface, or the dimensionless initial thickness of the lower electrolyte layer.

## 2.3. Assumptions and solution

We introduce the electroneutrality assumption for simplicity of analysis. Originally, this assumption was introduced by Planck [9], and the validity of the assumption has been verified numerically and experimentally for various electrochemical systems. For instance, Riveros [14] showed (for a somewhat different system) that the electroneutrality assumption is valid when  $\kappa_1 d > 20$ , where  $\kappa_1^{-1}$  is the Debye length for the dilute solution. This condition is readily satisfied for the present system of interest in which  $\kappa_1 d$  may normally be greater than  $10^2$ . Implication of the electroneutrality assumption is well interpreted by Mafé et al. [15,16], together with the in-depth perspectives concerning the charge-separation process and the condition under which the electroneutrality assumption holds.

Under the electroneutrality assumption, we let  $C_1 \cong C_2 = C$ . Then, the electromigration term in Eqs. (11a) and (11b) can be eliminated as follows. We multiply  $D_2$  and  $D_1$  by Eqs. (11a) and (11b) and add the resulting two equations together. This results in the following diffusion equation

$$\frac{\partial C}{\partial \tau} = \frac{\partial^2 C}{\partial \eta^2}. \quad (16)$$

Furthermore, by subtracting Eq. (11b) from Eq. (11a), and then rearranging the remaining terms, we obtain the dimensionless electric field  $\bar{E} = d\beta E$  as follows:

$$\bar{E} = -\frac{\partial \varphi}{\partial \eta} = \frac{1}{D_1 C_1 + D_2 C_2} \left( D_1 \frac{\partial C_1}{\partial \eta} - D_2 \frac{\partial C_2}{\partial \eta} \right), \quad (17)$$

which can be further simplified, by using the electroneutrality assumption, as

$$\bar{E} = \frac{D_1 - D_2}{D_1 + D_2} \frac{1}{C} \frac{\partial C}{\partial \eta} = (\alpha_1 - \alpha_2) \frac{1}{C} \frac{\partial C}{\partial \eta}, \quad (18)$$

where  $\alpha_i = D_i/(D_1 + D_2)$  is the transference number of each ionic species.

If we integrate Eq. (18), we obtain the following dimensionless potential distribution of

$$\varphi(\tau, \eta) = (\alpha_2 - \alpha_1) \ln \frac{C(\tau, \eta)}{C_1(\tau)} \quad (19)$$

and the dimensionless LJP of  $\bar{V}_{\text{LJP}} = \beta V_{\text{LJP}}$

$$\begin{aligned} \bar{V}_{\text{LJP}}(\tau) &= (\alpha_2 - \alpha_1) \ln \frac{C_h(\tau)}{C_1(\tau)} \\ &= 2.30(\alpha_2 - \alpha_1) \log \frac{C_h(\tau)}{C_1(\tau)}, \end{aligned} \quad (20)$$

where  $C_1 = C(\tau, 0)$  and  $C_h = C(\tau, 1)$ . Eq. (20) is a non-dimensional version of Planck's equation written for the finite domain of the present consideration. For an infinite domain  $C_1 = C_{10}$  and  $C_h = C_{h0}$  are constant, and therefore, the LJP is constant over time. For a finite domain both  $C_1$  and  $C_h$  are certainly dependent on time. Therefore, to determine the LJP, we should know  $C_1$  and  $C_h$  as functions of time.

If we substitute  $\partial \varphi / \partial \eta$  in Eq. (19) to the dimensionless Gauss equation of  $\partial \bar{E} / \partial \eta = \bar{\rho}_e$ , the dimensionless charge density  $\bar{\rho}_e = \rho_e(d^2\beta/\varepsilon)$  can be obtained as

$$\begin{aligned} \bar{\rho}_e &= (\alpha_1 - \alpha_2) \frac{\partial}{\partial \eta} \left( \frac{1}{C} \frac{\partial C}{\partial \eta} \right) \\ &= (\alpha_1 - \alpha_2) \frac{C''C - C'^2}{C^2}, \end{aligned} \quad (21)$$

where  $C' = \partial C / \partial \eta$  and  $C'' = \partial^2 C / \partial \eta^2$ .

The initial and the boundary conditions written for  $C_1$  and  $C_2$  are also satisfied by  $C$ . Then, the solution of Eq. (16), satisfying the initial and the boundary conditions of Eqs. (14) and (15), becomes (see Appendix A)

$$\begin{aligned} C(\tau, \eta; \xi) &= C_{h0} - \xi \\ &\quad - \frac{2}{\pi} \sum_{n=1}^{\infty} \frac{\sin n\pi\xi \exp(-n^2\pi^2\tau) \cos n\pi\eta}{n}, \end{aligned} \quad (22)$$

where  $C_{h0} = c_{h0}/(c_{h0} - c_{10})$ . From this, we can determine the concentrations at the lower and the upper walls, which become

$$C_1(\tau) = C_{h0} - \xi - \frac{2}{\pi} \sum_{n=1}^{\infty} \frac{\sin n\pi\xi \exp(-n^2\pi^2\tau)}{n}, \quad (23a)$$

$$\begin{aligned} C_h(\tau) &= C_{h0} - \xi \\ &\quad - \frac{2}{\pi} \sum_{n=1}^{\infty} \frac{(-1)^n \sin n\pi\xi \exp(-n^2\pi^2\tau)}{n}. \end{aligned} \quad (23b)$$

Additionally, the first and the second derivatives with respect to  $\eta$ , which are necessary to determine the electric field and the charge density, are obtained as

$$\begin{aligned} C'(\tau, \eta) &= 2(\alpha_1 - \alpha_2) \\ &\quad \times \sum_{n=1}^{\infty} \sin n\pi\xi \exp(-n^2\pi^2\tau) \sin n\pi\eta, \end{aligned} \quad (24a)$$

$$\begin{aligned} C''(\tau, \eta) &= 2\pi(\alpha_1 - \alpha_2) \\ &\quad \times \sum_{n=1}^{\infty} n \sin n\pi\xi \exp(-n^2\pi^2\tau) \cos n\pi\eta. \end{aligned} \quad (24b)$$

### 3. Results and discussions

#### 3.1. Concentration and electric field

Figs. 2 and 3 show the distribution of the concentration, the electrostatic potential, the electric field, and the charge density across the channel for the two cases of  $c_{h0}/c_{10} = 10^4$  and  $c_{h0}/c_{10} = 10$ , respectively. In each figure, the two initial interface positions of  $\xi = 0.5$  and  $\xi = 0.9$  are considered. In the figures, to eliminate the dependence of the results on the material, the electrostatic potential, the electric field, and the charge density are divided by the difference of the transference number,  $\alpha_1 - \alpha_2$ .

To check the validity of the analytical results, the numerical solution of Eq. (16) with the initial and boundary conditions of Eqs. (14) and (15) are obtained by a finite difference method. In the numerical analysis, the domain is discretized with 400 non-uniformly spaced node points, and the time step in the numerical calculation is fixed at  $\Delta\tau = 10^{-4}$  for all the calculations. Although this is not shown in the figure, the numerical solution and the analytical solution for the concentration distribution show almost perfect agreement.

It will be convenient to discuss the results by considering a rather specific case. We consider here the case of

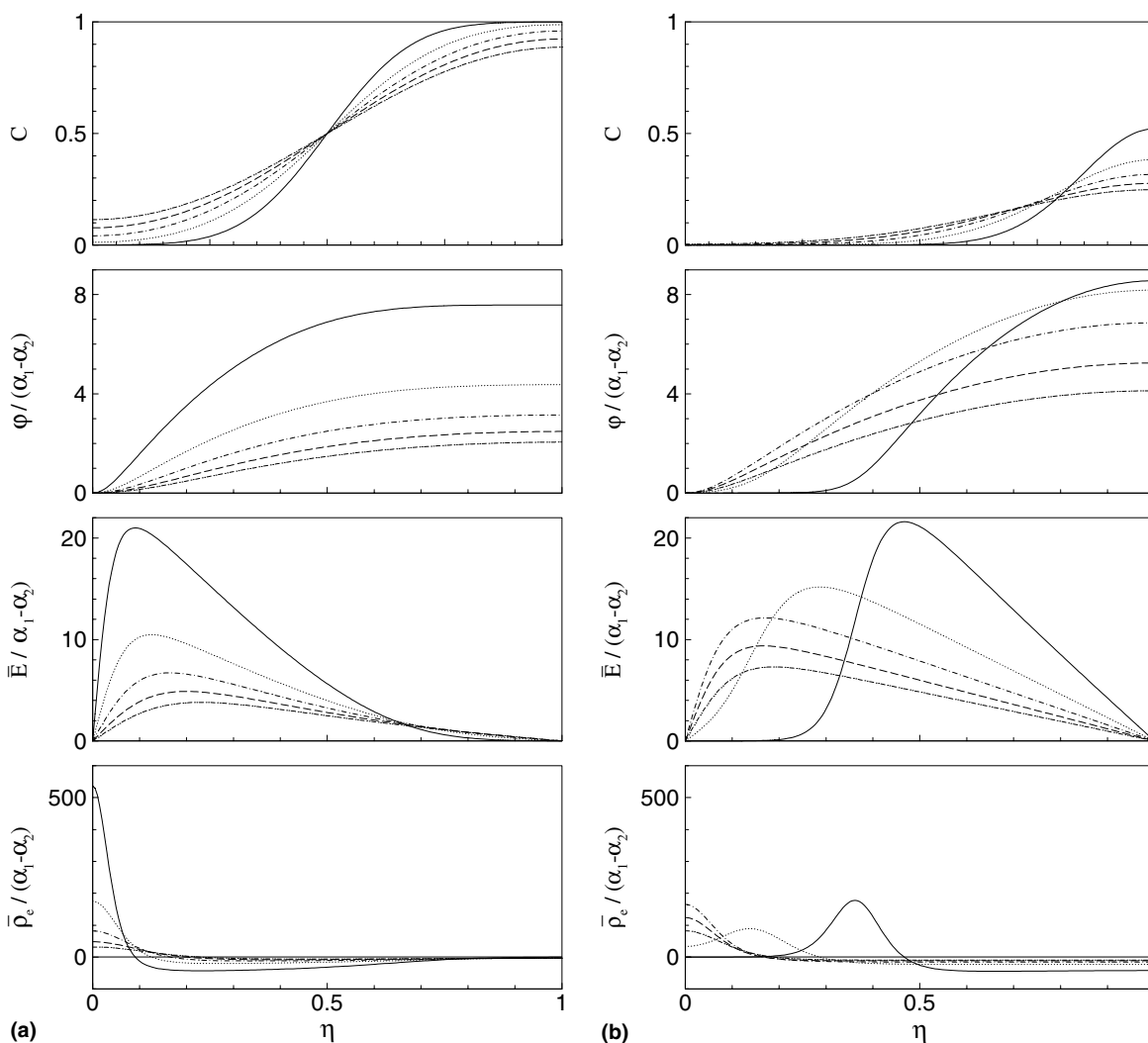


Fig. 2. Dimensionless concentration ( $C$ ) electrostatic potential ( $\phi$ ) electric field ( $\bar{E}$ ), and charge density ( $\bar{\rho}_e$ ) across the channel for the concentration ratio of  $c_{h0}/c_{l0} = 10^4$ : (a)  $\xi = 0.5$ ; (b)  $\xi = 0.9$ . The solid line, the dotted line, the dash-dot line, the dashed line, the dash-dot-dot line correspond to the results for  $\tau = 0.01, 0.02, \dots$ , and  $0.05$ , respectively.

aqueous NaCl solution. The diffusivities of  $\text{Na}^+$  and  $\text{Cl}^-$  ion in a dilute solution are  $1.33 \times 10^{-9}$  and  $2.03 \times 10^{-9}$   $\text{m}^2/\text{s}$ , respectively; thus  $D_{\text{eq}} = 1.607 \times 10^{-9}$   $\text{m}^2/\text{s}$  and  $\alpha_1 - \alpha_2 = -0.21$ . Since the value of  $\alpha_1 - \alpha_2$  is negative for the case of NaCl solution, the actual sign of the electrostatic potential, the electric field, and the charge density should be reversed with respect to those shown in Figs. 2 and 3. When  $d = 100$   $\mu\text{m}$ , for instance, the unity values of  $\phi/(\alpha_1 - \alpha_2)$ ,  $\bar{E}/(\alpha_1 - \alpha_2)$ , and  $\bar{\rho}_e/(\alpha_1 - \alpha_2)$  in Figs. 2 and 3 correspond to  $\phi = -5.4$  mV,  $E = -54$  V/m, and  $\rho_e = -3.72 \times 10^{-4}$  C/m<sup>3</sup> in dimensional values.

In Figs. 2 and 3, the charge density in the upper side of the channel is positive while it is negative in the lower side of the channel. When  $d = 100$   $\mu\text{m}$ , the charge density at the lower surface is about  $-0.2$  C/m<sup>3</sup> in dimensional value. This is because the diffusivity of  $\text{Cl}^-$  ion is greater than that of  $\text{Na}^+$  ion, so that  $\text{Cl}^-$  ion

diffuses towards the lower side more quickly. The electric field is always negative, that is, it is directed to the lower wall. Therefore, a downward Coulombic force acts on  $\text{Na}^+$  ion, while an upward Coulombic force acts on  $\text{Cl}^-$  ion. Consequently,  $\text{Na}^+$  ion will be accelerated and  $\text{Cl}^-$  ion will be decelerated, due to the action of the Coulombic force.

This has important practical implications in the transport of the charged particles, such as DNA and blood, in a microchannel. As manifested by Munson et al. [6], the mass transport across the microchannel can be promoted or suppressed by using the LJP. Therefore, the influence of the LJP and its electrophoretic contribution to a charged species should be properly accounted for in measuring the diffusion coefficient of the charged species in a T-sensor, and in systems that rely on tracking the spatial distribution of a species in a

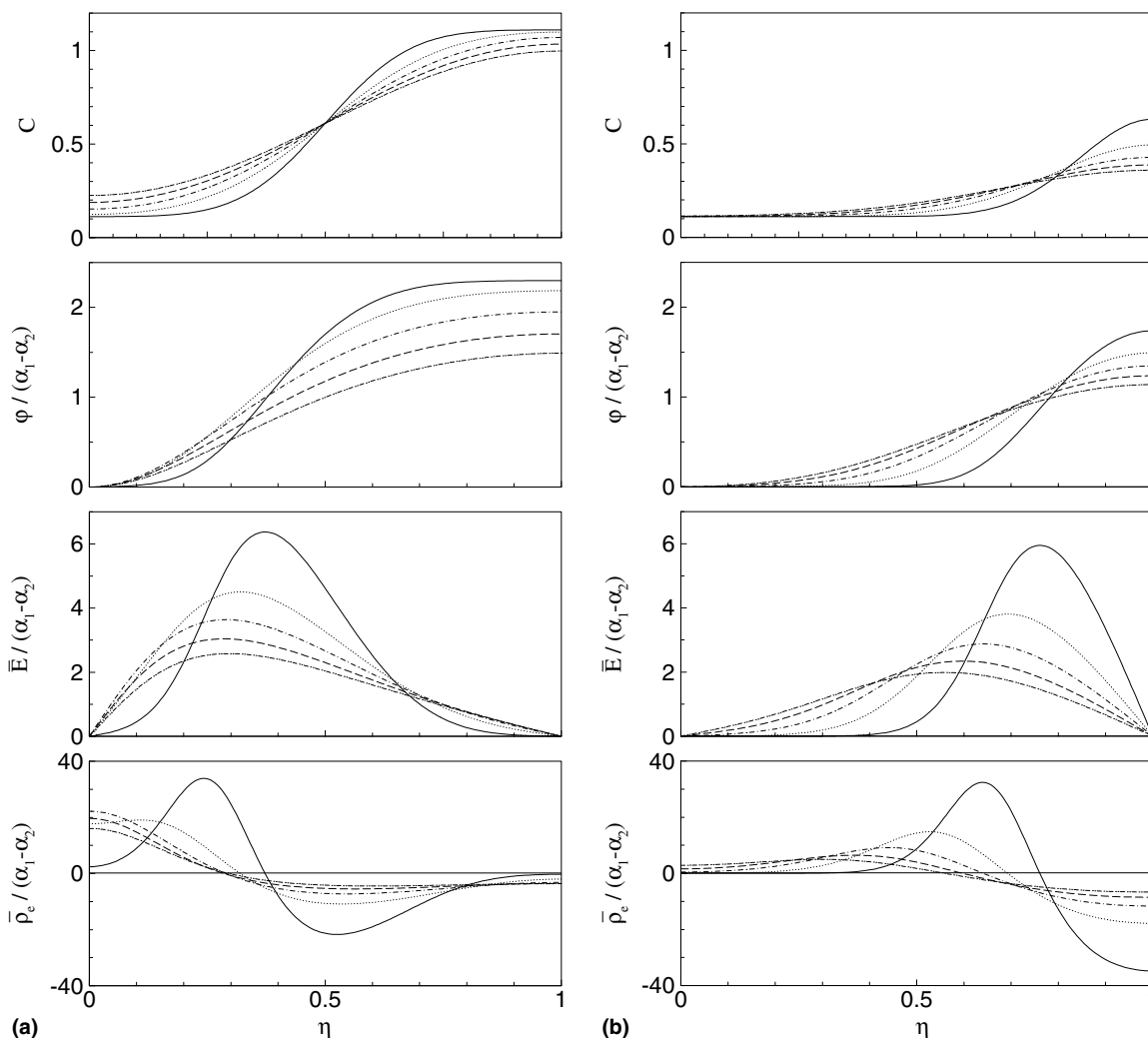


Fig. 3. Dimensionless concentration ( $C$ ) electrostatic potential ( $\varphi$ ) electric field ( $\bar{E}$ ), and charge density ( $\bar{\rho}_e$ ) across the channel for the concentration ratio of  $c_{h0}/c_{l0} = 10$ : (a)  $\xi = 0.5$ ; (b)  $\xi = 0.9$ . The solid line, the dotted line, the dash-dot line, the dashed line, the dash-dot-dot line correspond to the results for  $\tau = 0.01, 0.02, \dots$ , and  $0.05$ , respectively.

channel transverse to the direction of flow [6]. The present analytical prediction for the electric field will be helpful to assess the effect of the LJP in such problems.

Let us compare the results for the two cases of different initial interface positions in Figs. 2 and 3. When  $\xi = 0.9$ , the overall value of the concentration is rather smaller than those of  $\xi = 0.5$ . This is because a smaller amount of concentrated solution exists for the case of  $\xi = 0.9$ . On the other hand, differences in the overall value of the charge density, the electric field, and the electrostatic potential are not so significant between the two  $\xi$ s. This is because the number of polarized ions is in fact extremely small compared to the total number of ions in the channel. That is, the total polarized charge per unit length and unit depth of the channel is of the order of  $\varepsilon(dE/dy)d \sim \varepsilon E_{\max} = \varepsilon \bar{E}_{\max}/(d\beta)$ , while that of the total charge in the solution is of the order of  $Fcd$ . Thus, the ratio of the polarized charge with respect to

the total charge in the solution becomes  $\bar{E}_{\max}/(\kappa d)^2$ . It will be at most of the order of  $10^{-5}$ , even for micro-systems having the dimension of a few micrometers.

Next, we consider the effect of the initial concentration ratio  $c_{h0}/c_{l0}$  on the results, by comparing Figs. 2 and 3. Except for the concentration distribution, overall results for the case of  $c_{h0}/c_{l0} = 10^4$  show magnitudes roughly four times greater than those of  $c_{h0}/c_{l0} = 10^4$ . Considering that the initial concentration ratio is different by three orders, this is a rather small difference. This is because the concentration profile itself is only weakly dependent on the initial concentration. Therefore, if the initial concentration ratio is greater than a large value (say 100), only a minor difference exists in the temporal evolution of the concentration profile. Nevertheless, at initial times, however, the initial condition is dominating for the temporal evolution of all the variables; so that the LJP, the electric field and the

charge density will show logarithmic dependences on the initial concentration ratio.

### 3.2. Liquid junction potential

Fig. 4 shows the logarithmic value of the concentration ratio ( $\log C_h/C_l$ ) for the concentration ratio of  $c_{h0}/c_{l0} = 10, 10^2, 10^3$ , and  $10^4$ , in which  $\xi = 0.5$ . Since  $\beta^{-1} = 25.7$  mV, the LJP becomes (in dimensional form)

$$V_{LJP}(\tau)/\text{mV} = 59.1(\alpha_2 - \alpha_1) \log \frac{C_h(\tau)}{C_l(\tau)}. \quad (25)$$

At initial times, the LJP is logarithmically dependent on the initial concentration ratio. As discussed earlier,  $C_{h0} \rightarrow 1$  for a large initial concentration ratio, and then the concentration distribution in Eq. (22) will become

$$C(\tau, \eta; \xi) \rightarrow 1 - \xi - \frac{2}{\pi} \sum_{n=1}^{\infty} \frac{\sin n\pi\xi \exp(-n^2\pi^2\tau) \cos n\pi\eta}{n}. \quad (26)$$

Consequently, the concentrations at both walls will have the following limiting form

$$C_l(\tau) = 1 - \xi - \frac{2}{\pi} \sum_{n=1}^{\infty} \frac{\sin n\pi\xi \exp(-n^2\pi^2\tau)}{n}, \quad (27a)$$

$$C_h(\tau) = 1 - \xi - \frac{2}{\pi} \sum_{n=1}^{\infty} \frac{(-1)^n \sin n\pi\xi \exp(-n^2\pi^2\tau)}{n}. \quad (27b)$$

The limiting profile of the LJP, which is obtained by using Eqs. (27a) and (27b), is also drawn in Fig. 4. This limiting profile will lose its validity for the initial times. This is because  $C_{h0} = 1$  means that  $C_{l0} = 0$ ; accordingly,

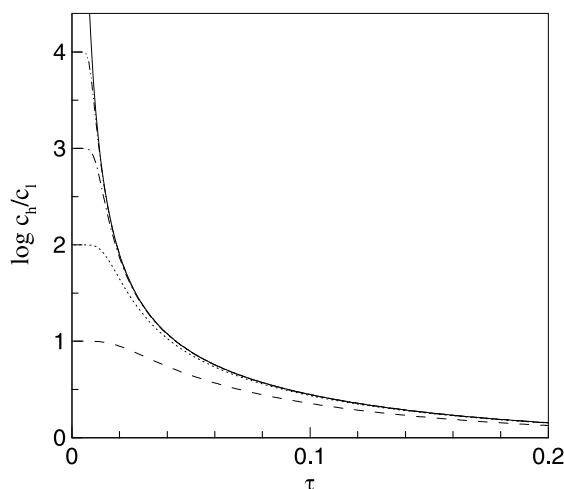


Fig. 4. Effect of the initial concentration ratio on the temporal evolution of the LJP. The dashed, dotted, dash-dot, and dash-dot-dot line are the results for  $c_{h0}/c_{l0} = 10, 10^2, 10^3$ , and  $10^4$ , respectively. The solid line corresponds to the limiting profile which is obtained by letting  $C_{h0} = 1$  and  $C_{l0} = 0$ .

the initial condition is dominating at the initial times, and then the LJP will diverge. It is shown in the figure that all the curves converge to the limiting profile after some transient period of time.

Fig. 5 shows the logarithmic value of the concentration ratio ( $\log C_h/C_l$ ) for various initial interface positions (i.e., the initial thickness ratios) for the concentration ratio of  $c_{h0}/c_{l0} = 10^4$ . At the initial times, all the results of  $\log C_h/C_l$  converge to  $\log C_{h0}/C_{l0} = 9.21$ . As shown in Fig. 5(a), except for the initial stage,  $\log C_h/C_l$  generally increases in proportion to  $\xi$ . In Fig. 5(b), the cases of  $\xi = 0.85, 0.9, 0.95, 0.99, 0.999$  are presented separately, which shows a similar result. As shown in Figs. 2 and 3 for the case of  $\xi = 0.5$  and  $0.9$ , the concentration difference between the top wall and the bottom wall is generally greater for the case of  $\xi = 0.5$ . However, since the concentration at the lower wall has in general a smaller value for the case of  $\xi = 0.9$ , therefore, the ratio of the concentration value

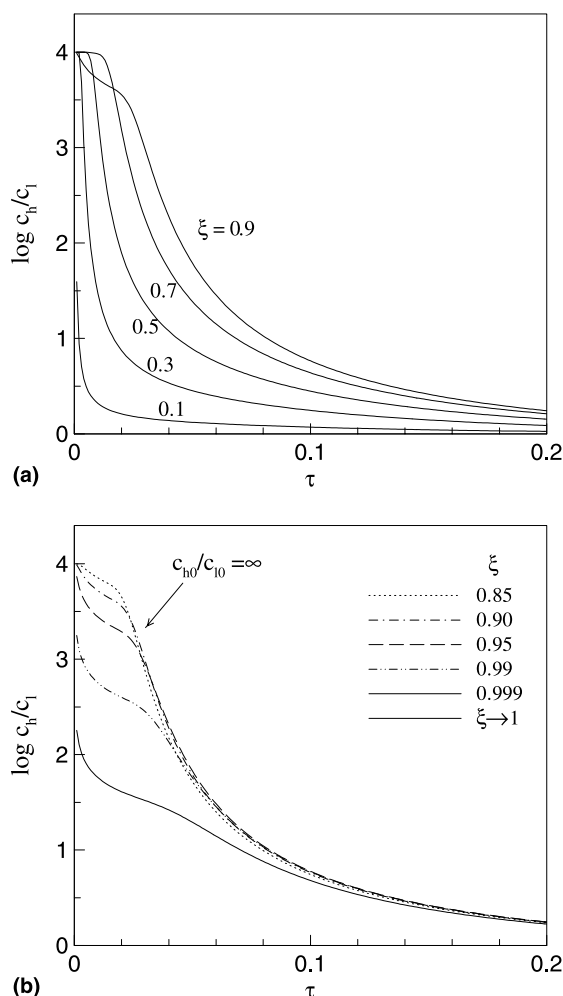


Fig. 5. Effect of initial thickness ratio of the electrolyte layers on the time evolution of the concentration ratio at both walls in which  $c_{h0}/c_{l0} = 10^4$ . The thicker line in (b) indicates the result for the limiting case of  $\xi \rightarrow 1$  and  $c_{h0}/c_{l0} = \infty$ .

of each wall (which is proportional to the LJP) is greater for the case of  $\xi = 0.9$ . This is because we have only a small amount of concentrated solution, and therefore, the mixing with the diluted solution near the interface will occur within a short period of time. Thus,  $\log C_h/C_l$  shows initially a fast decrease for the case of  $\xi = 0.9$ . Nevertheless, the concentration on the other side of wall is still very low because the diffusion from the top side to the bottom side will take a longer time for the case of  $\xi = 0.9$ .

This may have important practical implications for a fuel cell utilizing the concentration difference. In such a fuel cell, the fuel may be the concentrated salt water which can be produced by solar energy. The present result means that, after the initial period, we can obtain a higher open-circuit voltage by increasing  $\xi$ ; that is, with minimizing the fuel consumption.

Another interesting result is that, except for the initial stage of mixing, all the curves converge to almost a single curve in Fig. 5(b). To explain this trend, we consider a limiting case in which  $C_{h0} = 1$ ,  $C_{l0} = 0$ , and  $\xi \rightarrow 1$ ; that is, an infinitesimal but non-zero amount of concentrated electrolyte is present. Then, due to l'Hôpital's rule, it becomes

$$\lim_{\xi \rightarrow 1} \log \frac{C_h}{C_l} = \log \left. \frac{\partial C_h / \partial \xi}{\partial C_l / \partial \xi} \right|_{\xi=1} = \log \frac{1 + 2 \sum_{n=1}^{\infty} \exp(-n^2 \pi^2 \tau)}{1 + 2 \sum_{n=1}^{\infty} (-1)^n \exp(-n^2 \pi^2 \tau)}, \quad (28)$$

when  $\xi$  becomes exactly unity, which means the channel is filled with a homogeneous electrolyte, it will certainly become

$$C_l(\tau) = C_h(\tau) = C_{l0}$$

and the LJP has a zero value. It is clearly shown that all the curves in Fig. 5(b) converge to the limiting case of  $\xi \rightarrow 1$  except for the initial stage. This is certainly because the limiting formula in Eq. (28) is invalid near  $\tau = 0$ , since at that time  $C_l \cong 0$  and  $\log C_h/C_l$  will diverge.

Lastly, we compare the LJP of the present model with the existing experimental data. We use the experimental data obtained by the flowing electrochemical system of Josserand et al. [3]. Note that an analogy is satisfied between the present system under consideration and the flowing system if we make some simplifying assumptions [6]. In the diffusion problem of flowing systems, the streamwise diffusion (here,  $D_l \partial^2 c_i / \partial x^2$ ) is small. In addition, to the first order, we can let the velocity in the convection term (say,  $u_x(y) \partial c_i / \partial x$ ) be the mean velocity or the maximum velocity, depending on the problems. Then, if we replace the streamwise coordinate ( $x$ ) by the pseudo-time [6], we obtain an identical system of equations to Eqs. (5a), (5b) and (6).

Josserand et al. [3] have measured the LJP, when the two different concentrations of NaCl solutions flow in a

small rectangular channel, in a clever way. They reported the LJP for the two concentration ratios of  $c_{h0}/c_{l0} = 10$  and  $10^4$ . The flow velocity was the main parameter, and the electrode position (which was measured from the initial mixing point) was changed. The channel they used has a large aspect ratio to minimize the three-dimensional effect.

To compare with the present results, the results of Josserand et al. (Fig. 11 in [3]) are non-dimensionalized as follows:

$$\tau = \frac{D_{eq} x_e}{d^2 V}, \quad (29)$$

where  $x_e$  represents the electrode position (m),  $V$  the flow velocity (m/s), and  $d$  the channel width (m), in which  $x_e$  was  $10^{-2}$  and  $2 \times 10^{-2}$  m, and  $d$  was 2 mm in [3], respectively. The flow velocity was increased to about  $10^{-3}$  m/s.

Fig. 6 shows the comparison of the results. In the figure, the dotted line and the rectangular symbols are the theoretical and the experimental results for  $c_{h0}/c_{l0} = 10$ . The solid line and the circular symbols are the theoretical and the experimental results for  $c_{h0}/c_{l0} = 10^4$ . The two results obtained at different electrode positions are scaled well by the variables chosen in the present investigation (see Eq. (9)). Considering the simplification made for comparison, the present theory shows fairly good agreement to the experimental results for the flowing system. The case of  $c_{h0}/c_{l0} = 10^4$  shows better agreement to the experimental results. When  $\tau$  increases, the deviation between the experimental data and the present model increases, especially for the case of  $c_{h0}/c_{l0} = 10$ . Note that Fig. 6 is obtained by converting the data obtained for the flow velocity to the dimensionless time with Eq. (29). Thus, the data for small  $\tau$  were actually obtained for a greater

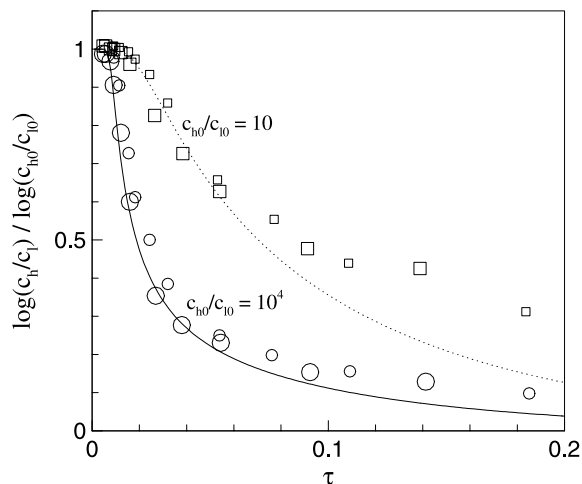


Fig. 6. Comparison of the theory with the experimental results of Josserand et al. [3]. The smaller symbols and larger symbols are obtained for different electrode positions of  $x_e = 10^{-2}$  m and  $2 \times 10^{-2}$  m in the paper of Josserand et al. [3].

flow velocity, and vice versa. It is unclear why the deviation is higher for the case of  $c_{h0}/c_{l0} = 10$  and for large  $\tau$ . A potential reason for such a deviation at low flow velocity (large  $\tau$ ) is an increase of relative significance of the streamwise diffusion which is not accounted for in the analysis.

We present the results for the scaled value of the LJP in Fig. 6. The original experimental results of Josseland et al. [3] show only a minor deviation from Planck's equation for a large velocity; that is, (in terms of  $\tau$ ) for small times. Considering that the present theory is consistent with Planck's equation, it is certain that the present theory also predicts the absolute value of the LJP.

#### 4. Conclusions

We have presented a theoretical modeling for the LJP for the two contacting fluids having different ionic concentrations in a slit-like two-dimensional channel. Theoretical formulas to predict the electric field, the LJP, and the charge density are derived in Eqs. (18), (20) and (21) by combining Planck's equation with the analytical solution of the concentration distribution. The theoretical results for the LJP are compared with the flowing electrochemical system, which shows a reasonable agreement.

The effect of the initial concentration ratio ( $c_{h0}/c_{l0}$ ) is investigated. At the initial stage of mixing, the overall values of the LJP, the electric field, and the charge density are logarithmically proportional to  $c_{h0}/c_{l0}$ . After a transient period of time, all the curves tend to converge to the curve representing the limiting condition of  $c_{h0}/c_{l0} = \infty$ .

Also considered is the effect of the initial thickness ratio ( $\xi$ ) of the dilute solution to the concentrated solution. After the initial time, the LJP has a greater value for higher values of the thickness ratios, which means the open-circuit voltage of the system will be greater when the thickness of the concentrated solution becomes smaller. It is shown that a limiting profile for the temporal evolution of the LJP exists in which  $c_{h0}/c_{l0} = \infty$  and  $\xi \rightarrow 1$ . Consequently, a maximum attainable open-circuit voltage exists (for the system considered in the present investigation) with respect to the variation of  $c_{h0}/c_{l0}$  and  $\xi$ .

#### Acknowledgements

The present investigation was supported by the Brain Korea 21 Program in 2002 and by the Pohang Steel Company (POSCO) Technology Development Fund in 2002 (Contract no. 1UD02013) administered by the Pohang University of Science and Technology. I.S.K. was also supported by a grant from the Korea Science and Engineering Foundation (KOSEF) (Contract no. R01-2001-00410).

#### Appendix A. Solution of diffusion equation

For the sake of convenience, we re-define the dimensionless concentration as follows:

$$C' = C - C_{l0}, \quad (\text{A.1})$$

where  $C_{l0} = c_{l0}/(c_{h0} - c_{l0})$ . Then, by introducing this to Eq. (16), we obtain

$$\frac{\partial C'}{\partial \tau} = \frac{\partial^2 C'}{\partial \eta^2}. \quad (\text{A.2})$$

The initial and the boundary conditions for  $C$  and  $\phi$  are written in dimensionless form as

$$C'(\tau = 0, \eta) = \begin{cases} 1 & \text{if } \eta < \xi, \\ 0 & \text{if } \eta > \xi, \end{cases} \quad (\text{A.3})$$

$$\left. \frac{\partial C'}{\partial \eta} \right|_{\eta=0} = \left. \frac{\partial C'}{\partial \eta} \right|_{\eta=1} = 0. \quad (\text{A.4})$$

The solution satisfying Eq. (A.2) and the boundary conditions of Eq. (A.4) can be obtained by separation of variables as

$$C'(\tau, \eta) = \sum_{n=1}^{\infty} b_n \exp(-n^2 \pi^2 \tau) \cos n \pi \eta. \quad (\text{A.5})$$

The unknown coefficient  $b_n$  is determined by using the initial condition of Eq. (A.3). That is, at initial time, it becomes

$$C'(\tau = 0, \eta) = \sum_{n=1}^{\infty} b_n \cos n \pi \eta = \begin{cases} 1 & \text{if } \eta < \xi, \\ 0 & \text{if } \eta > \xi. \end{cases} \quad (\text{A.6})$$

Then, we can obtain  $b_n$  by multiplying  $\cos n \pi \eta$  and then integrating both sides from  $\eta = 0$  to  $\eta = 1$ , as follows:

$$\begin{aligned} b_n &= 2 \int_0^1 C'(0, \eta) \cos n \pi \eta \, d\eta \\ &= - \int_0^{\xi} \cos n \pi \eta \, d\eta + \int_{\xi}^1 \cos n \pi \eta \, d\eta = - \frac{2}{n \pi} \sin n \pi \xi. \end{aligned}$$

In particular, when the thickness of the two layer is the same, i.e.,  $\xi = 1/2$ ,  $b_n$  becomes

$$c_n = \begin{cases} (-1)^{3(n+1)/2} \frac{2}{n \pi} & \text{if } n = 1, 3, 5, 7, \dots, \\ 0 & \text{otherwise.} \end{cases}$$

Applying the above  $b_n$  to Eq. (A.5), we obtain  $C'(\tau, \eta)$  as follows:

$$C'(\tau, \eta) = - \frac{2}{\pi} \sum_{n=1}^{\infty} \frac{\sin n \pi \xi \exp(-n^2 \pi^2 \tau) \cos n \pi \eta}{n} + b',$$

where  $b'$  is a constant. Then, it becomes

$$\begin{aligned} C(\tau, \eta) &= C_{l0} + C'(\tau, \eta) \\ &= b'' - \frac{2}{\pi} \sum_{n=1}^{\infty} \frac{\sin n \pi \xi \exp(-n^2 \pi^2 \tau) \cos n \pi \eta}{n}. \end{aligned} \quad (\text{A.7})$$

The unknown constant  $b'' = C_{10} + b'$  is determined from the requirement that the total amount of species should be constant at every instant. If we integrate  $C(\tau, \eta)$  from  $\eta = 0$  to  $\eta = 1$ , we obtain

$$b'' = C_{10}\zeta + C_{h0}(1 - \zeta) = C_{10} - \zeta.$$

Therefore, the mean concentration becomes

$$C(\tau, \eta; \zeta) = C_{h0} - \zeta - \frac{2}{\pi} \sum_{n=1}^{\infty} \frac{\sin n\pi\zeta \exp(-n^2\pi^2\tau) \cos n\pi\eta}{n}, \quad (\text{A.8})$$

where  $C_{h0} = c_{h0}/(c_{h0} - c_{10})$ .

## References

- [1] A.J. Bard, L.R. Faulkner, *Electrochemical Methods*, second ed., John Wiley & Sons, New York, 2001.
- [2] G. Lager, H. Jensen, J. Josserand, H.H. Girault, *J. Electroanal. Chem.* 545 (2003) 1.
- [3] J. Josserand, G. Lager, H. Jensen, R. Ferrigno, H.H. Girault, *J. Electroanal. Chem.* 546 (2003) 1.
- [4] R. Ferrigno, A.D. Strook, T.D. Clark, M. Mayer, G.M. Whitesides, *J. Am. Chem. Soc.* 124 (2002) 12930.
- [5] G. Borge, L.A. Fernández, J.M. Madariaga, *J. Electroanal. Chem.* 440 (1997) 183.
- [6] M.S. Munson, C.R. Cabrera, P. Yager, *Electrophoresis* 23 (2002) 2642.
- [7] C.H. Chen, J.G. Santiago, *Proc. 2002 Internal. Mech. Eng. Cong. and Exp.*, New Orleans, LA, CD 1, 2002, Paper no. 33563.
- [8] P.-A. Auroux, D. Iossifidis, D.R. Reyes, A. Manz, *Anal. Chem.* 74 (2002) 2637.
- [9] M. Planck, *Ann. Phys. Chem.* 40 (1890) 561.
- [10] H.J. Hickman, *Chem. Eng. Sci.* 25 (1970) 381.
- [11] J.L. Jackson, *J. Phys. Chem.* 78 (1974) 2060.
- [12] D.R. Hafeman, *J. Phys. Chem.* 69 (1965) 4226.
- [13] R.F. Probstein, *Physicochemical Hydrodynamics*, second ed., John Wiley & Sons, New York, 1994.
- [14] O.J. Riveros, *J. Phys. Chem.* 96 (1992) 6001.
- [15] S. Mafé, J. Pellicer, V.M. Aguilera, *J. Phys. Chem.* 90 (1986) 6045.
- [16] S. Mafé, J.A. Manzanara, J. Pellicer, *J. Electroanal. Chem.* 241 (1988) 57.